Article:
Liang, Xiaowen, Garcia, Brandon L., Visai, Livia et al. (5 more authors) (2016) Allosteric Regulation of Fibronectin/α5β1 Interaction by Fibronectin-Binding MSCRAMMs. PLoS ONE. 0159118. ISSN 1932-6203

https://doi.org/10.1371/journal.pone.0159118

PLOS ONE

RESEARCH ARTICLE

Allosteric Regulation of Fibronectin/$\alpha_5\beta_1$ Interaction by Fibronectin-Binding MSCRAMMs

Xiaowen Liang[1], Brandon L. Garcia[1¤a], Livia Visai[2,3], Sabitha Prabhakaran[1¤b], Nicola A. G. Meenan[4], Jennifer R. Potts[4], Martin J. Humphries[5], Magnus Höök[1]*

1 Center for Infectious and Inflammatory Diseases, Institute of Biosciences and Technology, Texas A&M Health Science Center, Houston, TX, 77030, United States of America, **2** Dep. of Molecular Medicine, UdR INSTM, Center for Tissue Engineering (C.I.T.), University of Pavia, 27100, Pavia, Italy, **3** Dep. of Occupational Medicine, Ergonomy and Disability, Salvatore Maugeri Foundation, IRCCS, Nanotechnology Laboratory, 27100, Pavia, Italy, **4** Department of Biology, University of York, York, YO10 5DD, United Kingdom, **5** Wellcome Trust Centre for Cell-Matrix Research, Faculty of Life Sciences, University of Manchester, Manchester, M13 9PT, United Kingdom

¤a Current address: Department of Biochemistry & Molecular Biophysics, Kansas State University, Manhattan, KS, 66506, United States of America
¤b Current address: Houston Methodist Hospital Research Institute, Houston Methodist Hospital, Houston, TX, 77030, United States of America
* mhook@ibt.tamhsc.edu

Citation: Liang X, Garcia BL, Visai L, Prabhakaran S, Meenan NAG, Potts JR, et al. (2016) Allosteric Regulation of Fibronectin/$\alpha_5\beta_1$ Interaction by Fibronectin-Binding MSCRAMMs. PLoS ONE 11(7): e0159118. doi:10.1371/journal.pone.0159118

Editor: Daniel Bouvard, Institut Albert Bonniot-INSERMU823, FRANCE

Received: May 7, 2016

Accepted: June 27, 2016

Published: July 19, 2016

Data Availability Statement: All relevant data are within the paper and its Supporting Information files.

Funding: This work was supported by NIH grants HL119648 and AI20624 to MH and AI113552 (to support BLG). This research was supported by the Wellcome Trust (072797) and the British Heart Foundation (FS/07/034). The funders had no role in study design, data collection and analysis, decision to publish, or preparation of the manuscript.

Competing Interests: The authors have declared that no competing interests exist.

Abstract

Adherence of microbes to host tissues is a hallmark of infectious disease and is often mediated by a class of adhesins termed MSCRAMMs (Microbial Surface Components Recognizing Adhesive Matrix Molecules). Numerous pathogens express MSCRAMMs that specifically bind the heterodimeric human glycoprotein fibronectin (Fn). In addition to roles in adhesion, Fn-binding MSCRAMMs exploit physiological Fn functions. For example, several pathogens can invade host cells by a mechanism whereby MSCRAMM-bound Fn bridges interaction with $\alpha_5\beta_1$ integrin. Here, we investigate two Fn-binding MSCRAMMs, FnBPA (*Staphylococcus aureus*) and BBK32 (*Borrelia burgdorferi*) to probe structure-activity relationships of MSCRAMM-induced Fn/$\alpha_5\beta_1$integrin activation. Circular dichroism, fluorescence resonance energy transfer, and dynamic light scattering techniques uncover a conformational rearrangement of Fn involving domains distant from the MSCRAMM binding site. Surface plasmon resonance experiments demonstrate a significant enhancement of Fn/$\alpha_5\beta_1$ integrin affinity in the presence of FnBPA or BBK32. Detailed kinetic analysis of these interactions reveal that this change in affinity can be attributed solely to an increase in the initial Fn/$\alpha_5\beta_1$ on-rate and that this rate-enhancement is dependent on high-affinity Fn-binding by MSCRAMMs. These data implicate MSCRAMM-induced perturbation of specific intramolecular contacts within the Fn heterodimer resulting in activation by exposing previously cryptic $\alpha_5\beta_1$ interaction motifs. By correlating structural changes in Fn to a direct measurement of increased Fn/$\alpha_5\beta_1$ affinity, this work significantly advances our understanding of the structural basis for the modulation of integrin function by Fn-binding MSCRAMMs.

Introduction

Fibronectin (Fn) is a multidomain glycoprotein found in blood plasma, other bodily fluids and the extra-cellular matrix (ECM) and serves as a natural ligand for several integrins including $\alpha_5\beta_1$, $\alpha_v\beta_3$, and $\alpha_4\beta_1$ [1]. The functional roles of Fn are diverse and include ECM assembly, angiogenesis, wound-repair, and oncogenesis [2]. Fn is secreted as a C-terminally disulfide-linked heterodimer composed of three structurally defined repeating units termed Fn domains or modules (Fig 1A). Major forms of Fn are comprised of 12 type I modules (FnI) and two type II modules (FnII), while splice variation results in 15 to 17 type III modules (FnIII). Fn is found in two predominant forms; cellular Fn, which is tissue localized and assembled into a fibrillar matrix, and the hepatocyte expressed, soluble plasma Fn that is secreted and maintained in blood at ~0.3 mg ml^{-1} [3]. Despite having independent functional roles from cellular Fn, it is significant that plasma Fn accounts for a large fraction of Fn found in tissue ECM [3,4].

To date, over one-hundred bacterial Fn-binding proteins (FnBPs) have been reported, and a majority of these belong to a protein family termed Microbial Surface Components Recognizing Adhesive Matrix Molecules (MSCRAMMs) [2]. Many Fn-binding MSCRAMMs contribute to virulence as *in vivo* studies demonstrate a critical role for these proteins in development of infectious diseases such as endocarditis, mastitis, and wound-infection [8–10]. A substantial body of evidence suggests that FnBPs can also manipulate physiological functions of Fn and thus contribute to pathogenesis in ways beyond mediating bacterial adhesion [6,11–16]. Indeed, several studies over the past decade involving the F1 and SfbI proteins from *Streptococcus pyogenes* [11,12,17], and more recently, BBK32 from *Borrelia burgdorferi* [6], have led to the development of a model whereby certain endogenous Fn activities are activated allosterically by Fn-binding MSCRAMMs. Specific intramolecular interactions exist in native plasma Fn which hold its solution conformation in a relatively compact state [18]. These interactions are mediated, in part, by FnI modules from the Fn-NTD fragment and FnIII modules originating from the distant Fn-CBD fragment (Fig 1A) [19–22]. Intrinsically disordered sequences from SfbI, F1, and BBK32 engage the Fn-NTD fragment via a tandem β-zipper model of binding [6,23–25] and, in doing so, compete for these intramolecular Fn contacts [6,12,24]. This competition results in a conformational expansion of Fn which has been directly measured using dynamic light scattering (DLS) upon binding of SfbI [12]. Interestingly, the SfbI-induced conformational change in Fn mirrors the transition of compact Fn to an elongated structure in solutions of increasing ionic strength [18].

A monoclonal antibody (mAbIII-10), which recognizes a conformationally-sensitive epitope within ^{10}FnIII [26] has also been used to monitor structural changes induced in Fn by both streptococcal and borrelial FnBPs [6,12,17]. These studies reveal a conformational rearrangement in Fn that occurs in domains located far outside of the FnBP/Fn binding site. The conformational expansion of Fn induced by binding of SfbI, F1, or BBK32 has been linked to three primary effects; (i) the 10th FnIII module of Fn which harbors the "RGD" integrin recognition motif exposes a previously cryptic mAbIII-10 epitope, (ii) the motogenic "IGD" motifs of the 7th and 9th FnI modules of the Fn-GBD fragment become exposed, and (iii) in the case of SfbI, binding results in the blocking of Fn assembly into fibrils. In addition to binding to the Fn-NTD fragment, SfbI, F1 and BBK32 also harbor an Fn-GBD binding site. However, Fn-NTD interaction alone is sufficient to induce allosteric changes in Fn [12]. Consistent with this is the recent discovery of the *Streptococcus equi* FnBP termed SFS, which only binds Fn via Fn-GBD interaction, yet fails to cause conformational expansion of Fn [27].

Integrins are essential metazoan heterodimeric glycoproteins that mediate cell-adhesion, establish transmembrane connections to the cytoskeleton, and play an integral role in cell

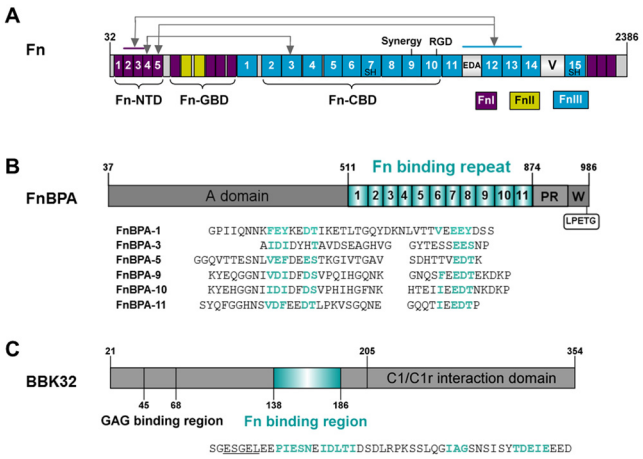

Fig 1. Domain architectures and sequences of the polypeptides. (**A**) Fn is a large C-terminally disulfide linked heterodimer that is modular in nature. Alternative splicing results in Fn monomers which are similar but not identical [5]. For clarity, only the larger monomer is shown here. Fn consists of three domain types each with distinct folds: FnI, FnII and FnIII (Uniprot ID: P02751). Splice variation results in a variable region (V) in a single Fn monomer. Several functionally relevant protease-stable Fn fragments are known, including the N-terminal domain (Fn-NTD), the gelatin-binding domain (Fn-GBD), and the cell-binding domain (Fn-CBD). The Fn-CBD fragment harbors the canonical $\alpha_5\beta_1$ "RGD" interaction motif within the 10th FnIII module and "synergy site" in the 9th FnIII module. Two free cysteines (SH) exist in each Fn monomer which were used to site-specifically label the FRET probes used in this study and are located in the 7th and 15th FnIII modules. Arrows indicate specific intramolecular interactions formed between domains of the Fn-NTD fragment and the distant Fn-CBD fragment. (**B**) Domain organizations of mature FnBPA from *S. aureus*. The extracellular region of FnBPA consists of an A domain that interacts with fibrinogen, followed by a sequential arrangement of 11 Fn binding repeats, the proline-rich (PR) and cell wall (W) spanning regions, and a C-terminal sortase A recognition motif (LPETG) (Uniprot ID: P14738). Sequence alignment of Fn-binding repeats used in this study are shown. Highlighted in cyan are the residues within each repeat that bind to or are presumed to engage Fn-NTD. (**C**) Domain organizations of mature BBK32 from *B. burgdorferi* (Uniprot ID: O50835). The residues involved in binding to Fn-NTD are shown in cyan. Unlike FnBPA BBK32 also encodes a binding site for Fn-GBD indicated by the underlined sequence [6]. The recently identified C1 binding domain is also indicated [7]. All domains are drawn to the scale using IBS (Illustrator for Biological Sequences, http://ibs.biocuckoo.org).

doi:10.1371/journal.pone.0159118.g001

signaling pathways [28]. Interestingly, integrins are common targets of pathogens and often participate in bacterial and viral adhesion to host cells [29]. Two modes of microbial integrin recognition have been described and include direct binding by bacterial surface proteins [30–32] or indirect binding via physiological ligands such as Fn [29,33,34]. The latter mode is exemplified by an FnBP expressed by the gram-positive pathogen *Staphylococcus aureus*, termed FnBPA [35]. By acting as a molecular bridge, staphylococcal FnBPA exploits Fn's role as a natural substrate for $\alpha_5\beta_1$ integrin, causing activation of endocytic pathways, and ultimately resulting in the internalization of *S. aureus* by non-professional phagocytes [14–16,36–45]. Full-length FnBPA harbors eleven Fn-binding repeats that specifically interact with the $^{2-5}$FnI modules of the Fn-NTD fragment via a tandem beta-zipper [25,46] (Fig 1B). Unlike the streptococcal and borrelial FnBPs, FnBPA binds exclusively to Fn-NTD and makes no direct interactions with the Fn-GBD fragment. Of the 11 FnBPA Fn-binding repeats, six exhibit high-affinity binding of Fn [46] and a single high-affinity repeat is sufficient for $\alpha_5\beta_1$ integrin-dependent *in vitro* invasion of endothelial cells by *S. aureus* [14].

While *S. aureus* is typically considered an extracellular pathogen, intracellular *S. aureus* is associated with several chronic and reoccurring infections [47–50] and can establish infection even in the presence of the vancomycin [51]. Thus, *S. aureus* internalized by non-professional phagocytes represents a bacterial reservoir protected against antibiotics and innate host defense

systems. Although it is evident that FnBPA, Fn, and $\alpha_5\beta_1$ integrin work in concert to promote an intracellular "life-style" for *S. aureus* [14–16,40], detailed knowledge of the underlying molecular events that lead to invasion have remained elusive. A mechanistic understanding of how FnBPA manipulates Fn function to enable entry of *S. aureus* into non-phagocytic cell types, will benefit renewed efforts [51] to target this form of the pathogen. With this in mind, the goals of this study were to determine if the allosteric model of Fn activation, which has been proposed for streptococcal and borrelial FnBPs, applies to staphylococcal FnBPA. Furthermore, we sought to better understand the nature of structural changes induced by Fn-binding MSCRAMMs and correlate these changes to quantitative and direct measurements of Fn/$\alpha_5\beta_1$ integrin interaction. Therefore, in parallel with our studies of FnBPA, we have also evaluated the effect of borrelial BBK32 (Fig 1C) on the solution structure of Fn and its effect on Fn/$\alpha_5\beta_1$ interaction. Herein, we apply a cross-disciplinary approach to dissect the structural basis for MSCRAMM-induced Fn activation using circular dichroism (CD), DLS, and fluorescence resonance energy transfer (FRET) to examine the conformational status of native Fn or MSCRAMM-bound Fn in solution. Surface plasmon resonance (SPR) is used to quantitatively measure the effects of FnBPA and BBK32 on direct Fn/$\alpha_5\beta_1$ interaction. Together these experiments provide a detailed structure-activity relationship of MSCRAMM/host interaction and strongly suggest an allosteric mode of Fn/$\alpha_5\beta_1$ affinity-enhancement for Fn-binding MSCRAMMs.

Materials and Methods

Materials

Human Fn was purified from freshly drawn citrated plasma (Gulf Coast Regional Blood Center, Houston, TX) using gelatin affinity chromatography combined with arginine affinity chromatography as described previously [52]. Fn was stored at 4°C in Tris-buffered saline (TBS: 50 mM Tris-HCl, pH 7.4, 150 mM NaCl), and used within one month. Fn dimer concentration was calculated from OD_{280} nm with EC_{280} (1%) = 12.8 and molecular weight of 500 kDa. The ectodomain of integrin $\alpha_5\beta_1$-Fc fusion protein, which contains the N-terminal 613 residues of α_5-subunit and fragment 121–455 of β_1-subunit, was generated and purified as previously reported [53]. Fn-NTD and Fn-CBD were purified as previously described [54]. Expression and purification of recombinant GST-FnBPAs, FnBPA-10 peptide and $BBK32_{(21–205)}$ was performed as previously described [46,55]. Rabbit anti-Fn pAb (polyclonal antibody) was purchased from ICN Pharmaceuticals, Inc. (Costa Mesa, California). BSA (bovine serum albumin), heparin sodium (from porcine intestinal mucosa, 17,000–19,000 Da) was from Sigma.

Dynamic light scattering

DLS measurements were performed using DynaPro Titan Ambient laser unit (Wyatt Technology Corporation) with wavelength at 828.5 nm and 10% to 12% laser power. Samples were dissolved in TBS and filtered through 0.22 μm filter to eliminate any particles. Fn concentration was maintained at 0.8 mg ml^{-1} (1.6 μM as dimer) in TBS (50 mM Tris-HCl pH 7.4, 150 mM NaCl) for the conditions tested. After equilibration at room temperature for 15 to 30 min, the samples were measured three times, with each measurement lasting 100 seconds (10 acquisitions, 10 seconds each). Data analysis was performed using Dynamics V6 software.

Circular Dichroism

CD measurements in the near UV region (350–250 nm) were carried out at ambient temperature on a Jasco J-720 spectropolarimeter (Easton, MD) with a 1 cm cell. Ten scans were

collected and averaged at a scan speed of 200 nm min^{-1}, with a time constant of 1 s and band width of 1 nm. A mean residue molecular weight of 110 was used in the calculation of mean residue ellipticity. The spectra of the Fn solution were background-corrected with the CD signal obtained from the buffer or molecules mixed with Fn.

Fluorescence resonance energy transfer

Fluorescence labeling of human plasma Fn was performed at room temperature as described previously [56]. The fluorescence probes used in this study were purchased from Molecular Probes. Briefly, newly purified human plasma Fn at 1.2 mg ml^{-1} in TBS was partly denatured in 4 M GdnHCl (Sigma) for 15 min to expose the free cysteines in the Fn dimer. The denatured Fn was mixed with thiol-reactive Alexa Fluo® 546 C5-maleimide (AF546, ~15-fold molar excess over Fn monomer concentration) and allowed to incubate for 2 hr with gentle rocking. The acceptor fluorophore AF546-conjugated Fn (~0.9 mg ml^{-1}) was labeled with a second probe, the amine-reactive Alexa Fluo® 488 carboxylic acid-succinimidyl ester-mixed-isomers (AF488, ~20-fold molar excess). After each labeling, the unbound dye was removed using a PD-10 desalting column (GE Healthcare). The labeling ratios were ~8 AF488 donors and ~4 AF546 acceptors in each Fn dimer.

FRET within donor and acceptor-labeled Fn was measured using spectrofluorimeter LS 50B (Perkin-Elmer) at room temperature with excitation wavelength at 493 nm. The sensitivity of FRET response to the Fn unfolding was evaluated under mild denaturant (up to 2 M guanidinium chloride (GdnHCl)). Measurement of MSCRAMM-induced FRET within Fn was performed by titrating 0.5, 2 and 5 μl of 50 μM of BBK32 or FnBPA-10 in to 500 μl of labeled Fn. Subsequently, the emission spectra collected for each titration was recorded and normalized to the donor emission peak so that changes in energy transfer were reflected only by changes in the acceptor peak. Control experiments were conducted using an equimolar solution of donor-labeled Fn with acceptor-labeled Fn in the presence and absence of 2M GdnHCl to confirm the absence of energy transfer between adjacent Fn molecules in solution.

SPR-based Biacore analysis of Fn and $\alpha_5\beta_1$ interaction

Experiments were performed at 25°C on a Biacore 3000 (GE Healthcare Bio-Sciences AB, Uppsala, Sweden) using HBS-T (10 mM HEPES, pH 7.3, 150 mM NaCl, 0.005% Tween-20) containing 1 mM $MnCl_2$. To prepare sensor surface for kinetic experiments, ~1400 RU of $\alpha_5\beta_1$ was immobilized to a CM5 chip by amine coupling. Briefly, 18 μL of protein (10 μg ml^{-1} in 10 mM sodium acetate, pH 4.8) was injected onto an activated (4 min activation) surface at a flow rate of 5 μl min^{-1}. BSA was coupled to the adjacent flow cell and served as a reference surface (~5000 RU). A flow rate of 30 μL min^{-1} was used for all binding experiments. The sensor chip surface was regenerated to remove bound Fn by injection of 1 M NaCl for 1 min. All measurements were baseline corrected by subtracting the response from the reference surface. For kinetic analysis, signals from buffer blanks were subtracted.

Kinetic constants were obtained from curve fitting to the predefined bivalent analyte model using BIAevaluation software (Version 4.1). Heterodimeric Fn has two identical binding sites for integrin $\alpha_5\beta_1$. The reaction between soluble Fn analyte (A) and immobilized integrin ligand (L) can be described by this equation:

$$A + L \underset{k_{d1}}{\overset{k_{a1}}{\leftrightarrow}} AL + L \underset{k_{d2}}{\overset{k_{a2}}{\leftrightarrow}} AL_2$$

Binding to the first ligand molecule is described by a single set of rate constants (k_{a1}, k_{d1}), so that the two sites on the analyte are equivalent in the first binding step. Binding of the second

ligand molecule is described by a second set of rate constants (k_{a2}, k_{d2}), which is reported in an unconventional units of $RU^{-1}s^{-1}$. The first set of rate constants were used for calculating the dissociation constant K_D ($K_D = k_{d1}/k_{a1}$).

ELISA-type binding assays

Experiments were conducted at room temperature and each sample was assayed in triplicate. Immunoassay microplate Immulon 2HB (Thermo Scientific, Waltham, MA) was coated with 2 μg of integrins dissolved in TBS for 1 hour. The plate was then blocked for 1 h with 1% (w/v) BSA in a buffer "A" (TBS containing 1 mM $MnCl_2$). Citrated plasma (stored at -20°C for less than 6 months) was fast-thawed at 37°C and spun to remove aggregates. The supernatant was diluted 10-fold in buffer "A" and then mixed with varying concentrations of BBK32 to a final concentration of 5% plasma. The sample mixtures were added onto the plate and incubated for 1 h. The plate was washed three times with buffer "B" (TBS with 1 mM, $MnCl_2$, and 0.05% Tween-20) before addition of rabbit anti-Fn antibody. Following washing with buffer "B", AP-conjugated goat-anti-rabbit IgG (BioRad, Hercules, CA) was added to the plate and incubated for 1 h. All antibodies were diluted 2000-fold in buffer "B" containing 1% BSA. Alkaline phosphatase substrate PNPP (Pierce, Rockford, IL) was added after washing, and the absorbance was measured at 405 nm using a Thermo Max plate reader (Molecular Devices, Sunnyvale, CA).

Results

The tertiary structure of plasma Fn is altered by FnBPA and BBK32

Although high resolution crystal structures have been solved for a number of smaller Fn fragments, a complete structure of full-length Fn remains to be determined. However, a wide range of biophysical studies using DLS [18,57–61], CD [59,62,63], steady-state fluorescence spectroscopy [59,63,64], small-angle X-ray scattering (SAXS) [65] and small-angle neutron scattering (SANS) [60,65,66] have yielded a wealth of information about the conformational states and structure of native Fn in solution. Conformational changes induced by FnBPs underlie the allosteric model of Fn activation proposed for streptococcal and borrelial FnBPs [6,12,17], and a previous study using DLS indicates an expansion of Fn structure upon SfbI binding which is similar to what is observed when Fn is incubated in a high salt medium [12]. To understand if analogous conformational changes are induced by staphylococcal FnBPA we used DLS to measure the hydrodynamic radii (R_h) of Fn in the presence or absence of the FnBPA Fn-binding repeat FnBPA-10 (Table 1). Fn adopted an extended conformation in the presence of high salt

Table 1. Comparison of hydrodynamic radii of Fn under various conditions.

Fn treatments	R_h (nm)
TBS	10.20 ± 0.12
High salt	13.27 ± 0.15
Heparin	12.50 ± 0.29
FnBPA-10	12.73 ± 0.69
BBK32	13.00 ± 0.38

Dynamic light scattering measurements were performed using DynaPro Titan Ambient laser unit. Fn was maintained in TBS at a final concentration of 0.8 mg ml^{-1} (1.6 μM) for the conditions tested. Different treatments are additional 350 mM NaCl (high salt), 15 μM of heparin, FnBPA-10 peptide, or 6 μM of BBK32 recombinant protein. Values are mean ± SE obtained from a minimum of three independent experiments.

doi:10.1371/journal.pone.0159118.t001

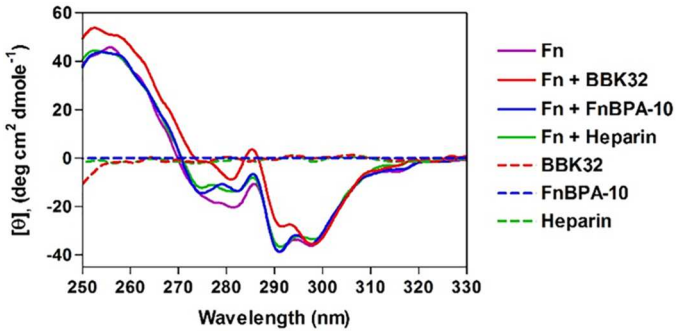

Fig 2. Near-UV CD spectra of Fn. CD spectra in the range of 250–350 nm are shown for individual molecules or mixtures: Fn dimer (0.82 mg ml^{-1}, 1.6 μM), BBK32 (0.14 mg ml^{-1}, 6.0 μM), FnBPA-10 (0.07 mg ml^{-1}, 15 μM), and heparin (0.27 mg ml^{-1}, 15 μM). All concentrations are final. TBS (50 mM Tris-HCl pH 7.4, 150 mM NaCl) was used for all experiments.

doi:10.1371/journal.pone.0159118.g002

or heparin (R_h = 13.27 ± 0.15; 12.50 ± 0.29, respectively) compared to a more compact structure found in physiological buffer (R_h = 10.20 ± 0.12) which is consistent with previous measurements of Fn R_h by DLS [12,18]. Addition of staphylococcal FnBPA-10 (R_h = 12.73 ± 0.69) or the borrelial FnBP, BBK32 (R_h = 13.00 ± 0.38) resulted in a significantly increased R_h, suggesting that Fn indeed adopts an extended structure upon binding to these MSCRAMMs.

Native Fn contains large numbers of aromatic residues in its type I and III domains which exist in common hydrophobic environments and give rise to a signature near-UV CD spectrum characterized by two strong negative peaks centered at 291 nm and 299 nm, and a weaker negative peak at 282 nm (Fig 2) [67,68]. Binding of Fn by the glycosaminoglycan heparin has been shown to alter Fn tertiary structure which can be monitored by shifts in this signature spectrum (Fig 2) [69]. When Fn was incubated in the presence of FnBPA-10 or BBK32, both complexes produce significantly different spectra relative to native Fn (Fig 2). Interestingly we noted the similarity in the near-UV spectra for heparin-bound Fn when compared to FnBPA-10/Fn (Fig 2), whereas, the BBK32 spectrum is reminiscent of the partial unfolding of Fn in 4M urea [63]. Importantly, the MSCRAMM fragments used in these experiments are intrinsically disordered polypeptides that do not contain tryptophan residues and therefore lack near-UV optical activity [70] (Fig 2). However, since the Fn-NTD is engaged by BBK32 and FnBPA-10, such interaction could potentially cause near-UV CD optical activity changes within NTD domain. As shown in S1 Fig, BBK32 and FnBPA-10 caused intrinsic Trp fluorescence quenching in Fn (S1A Fig) and Fn-NTD (S1B Fig), suggesting that Trp environments in the NTD and GBD (in the case for BBK32) are affected by the binding and may attribute partially to the near-UV CD changes in Fn.

Data obtained using an anti-Fn antibody (mAb10-III) that recognizes a conformational sensitive epitope indicates that structural changes distant from the streptococcal and borrelial FnBP binding site are induced in Fn [6,12,17] on MSCRAMM binding. To learn if FnBPA causes similar allosteric changes in Fn upon binding, and to confirm apparent conformational changes in solution Fn indicated by CD (Fig 2), we next employed a FRET-based approach. To this end, Fn was site-specifically labelled by conjugating an acceptor fluorophore to free cysteine residues using a technique previously described [56]. Native Fn contains only two free cysteines (4 per dimer molecule) and these are found in the C-terminally positioned ^{7}FnIII and ^{15}FnIII modules [71] (denoted in Fig 1A). When Fn is denatured by introducing increasing amounts of GdnHCl (Fig 3A and 3B), or incubated in the presence of increasing ionic strength (Fig 3C), the distance between the amine coupled donor fluorophores and the cysteine coupled acceptor fluorophores increased and the acceptor peak was diminished. There is not FRET

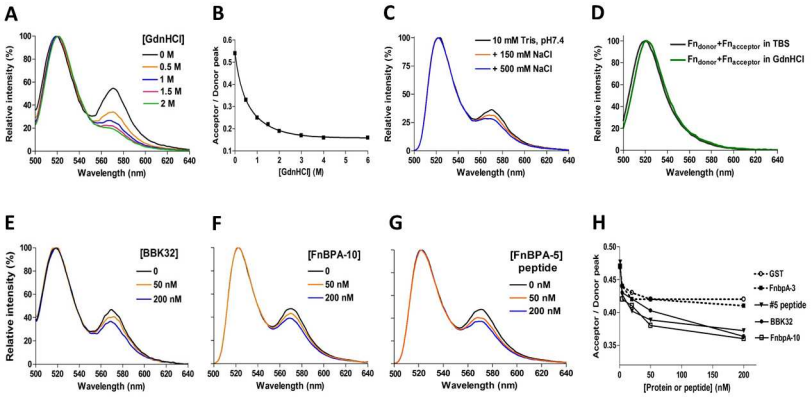

Fig 3. Fluorescent resonance energy transfer of Fn. Fluorescence emission spectra of Fn-D/A (50 nM in 10 mM Tris, pH7.4, 150 mM NaCl) were collected at 493 nm excitation, (A) in the presence or absence of denaturant (GdnHCl) and (B) accompanying Acceptor/Donor peak ratio as a function of denaturant concentration. Fn-D/A fluorescence emission changes (C) under different ionic strengths, and (E-G) in the presence of different concentrations of BBK32, GST-FnBPA-10, or FnBPA-5 peptide. (H) Acceptor/Donor peak ratio vs. concentration (0, 1, 5, 20, 50 and 200 nM) of protein or peptide added. Spectra are normalized to the donor emission peak at 522 nm such that changes in energy transfer are reflected only by changes in the acceptor peak at 570 nm. (D) Control experiments were conducted by mixing 50 nM of donor-labeled Fn (Fn_{donor}) with 50 nM of acceptor-labeled Fn ($Fn_{acceptor}$) in TBS or 2 M GdnHCl.

doi:10.1371/journal.pone.0159118.g003

observed between adjacent or denatured Fn molecules (Fig 3D). To determine if the MSCRAMM-induced structural changes measured by CD and DLS involve Fn domains outside of the MSCRAMM binding site, spectra were then collected in the presence of various concentrations of BBK32 (Fig 3E) and FnBPA-10 (Fig 3F) GST fusion proteins. These experiments showed a clear dose-dependent loss of acceptor peak signal for MSCRAMM-bound Fn. Importantly, an identical effect is observed when a 36 amino acid peptide lacking the GST fusion and corresponding to the high-affinity FnBPA repeat FnBPA-5 is used (Fig 3G). GST alone or a GST fusion to the low-affinity FnBPA repeat FnBPA-3 exhibits no effect in this assay system (Fig 3H). Taken together, the DLS, CD, and fluorescence based assays indicated that BBK32 and FnBPA profoundly modify the native solution structure of Fn by promoting an extended Fn conformation that results in large scale rearrangement of Fn domains at sites distant from the MSCRAMM binding site.

Fn recognition of the $\alpha_5\beta_1$ integrin is enhanced by FnBPA and BBK32

Fn serves as a primary ECM substrate for several adhesion molecules including the major Fn cell surface receptor, $\alpha_5\beta_1$ integrin [1]. We hypothesized that conformational changes induced upon binding by FnBPA or BBK32, as shown in Figs 2 and 3 and Table 1, may result in modified Fn/integrin interactions. Previous studies on streptococcal and borrelial Fn-binding MSCRAMMs have used the conformational Fn antibody (mAb10-III) as a surrogate for potential effects on Fn/$\alpha_5\beta_1$ integrin interaction. To test this more directly, we developed an SPR-based system to study the effects of FnBPA and BBK32 on the recognition of $\alpha_5\beta_1$ integrin by Fn. Briefly, a recombinant $\alpha_5\beta_1$-Fc fusion protein representing the minimal functional unit of the integrin [53] was immobilized on the surface of a Biacore CM5 chip. Fn interacts with the $\alpha_5\beta_1$ biosensor and binding is enhanced by Mn^{2+} as previously reported (S1A Fig) [53]. Further validation of this experimental approach was performed by using Fn fragments including the cell-binding domain (Fn-CBD) possessing the canonical $\alpha_5\beta_1$-binding "RGD" (^{10}FnIII) and PSHRN synergy sites (^{9}FnIII) [72,73]. As expected, the Fn-CBD fragment exhibited dose-

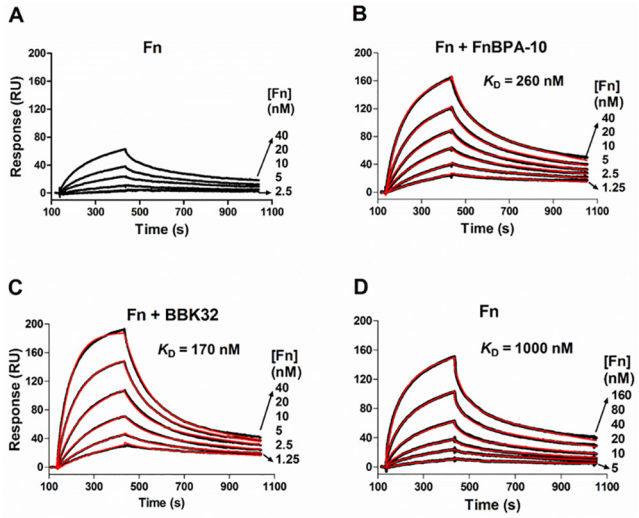

Fig 4. SPR analysis of direct Fn/$\alpha_5\beta_1$ interaction in the presence of Fn-binding MSCRAMMs. (A) Two-fold linear dilution series of Fn in HBS-T containing 1 mM $MnCl_2$, and in the presence of **(B)** 1 μM of FnBPA-10, or **(C)** 0.5 μM of BBK32 were injected over the $\alpha_5\beta_1$ biosensor. **(D)** A higher Fn concentration series was used for measurement of Fn/$\alpha_5\beta_1$ binding kinetics in the absence of MSCRAMMs. The SPR response curves generated from Fn binding to $\alpha_5\beta_1$ are shown in black with lower curve corresponding to lower concentration of Fn injected. Dissociation constants (K_D) for Fn/$\alpha_5\beta_1$ the interaction **(B-D)** were obtained from fitting SPR response curves to a bivalent analyte binding model (fitted lines are shown in red) and the kinetic parameters are listed in Table 2. There was no detectable binding when FnBPA-10 (1 μM) or BBK32 (0.5 μM) were injected over the same $\alpha_5\beta_1$ surface (data not shown).

doi:10.1371/journal.pone.0159118.g004

dependent interaction with $\alpha_5\beta_1$, while the Fn-NTD fragment lacking the integrin interaction domains failed to bind the integrin (S1B and S1C Fig).

Using this approach we measured a moderate affinity of ~1 μM for Fn/$\alpha_5\beta_1$ (Fig 4A–4D) that is in good agreement with affinities reported for fibroblast cell interaction with plasma Fn [74]. To understand if MSCRAMM binding to Fn affects the Fn/$\alpha_5\beta_1$ interaction, we next injected mixtures of BBK32/Fn or FnBPA-10/Fn (fixed MSCRAMM + varied Fn concentrations) over the immobilized $\alpha_5\beta_1$ integrin. A remarkable enhancement of the binding response was observed for MSCRAMM-bound Fn relative to native Fn (Fig 4B–4D). To obtain a quantitative measure of the increase in affinity, kinetic parameters were obtained by fitting SPR response curves to a bivalent analyte binding model (Fig 4B–4D). This model was selected on the basis of closeness of fit ($\chi^2 \approx 1$, Table 1) and the expectation that dimeric Fn contributes one identical $\alpha_5\beta_1$ binding site per subunit. Analysis for each interaction revealed that the approximately five-fold increase in apparent affinity (K_D) ($K_D^{Fn/\alpha5\beta1}$ = 1000 nM vs. $K_D^{BBK32/Fn/\alpha5\beta1}$ = 170 nM & $K_D^{FnBPA\text{-}10/Fn/\alpha5\beta1}$ = 260 nM) was due to an increase in the initial association rate ([k_{a1} = (1.5, 6.1, & 7.5) x10^4 $M^{-1}s^{-1}$], respectively). Interestingly, all other rate constants (k_{d1}, k_{a2} and k_{d2}) (Table 2) were similar across experiments, indicating that the Fn/$\alpha_5\beta_1$ binding site present in native Fn is the same for MSCRAMM-bound Fn.

To address the specificity of enhanced Fn/$\alpha_5\beta_1$ activity and to further dissect the kinetic observations presented above, we next injected a mixture of varied MSCRAMM and fixed Fn concentrations (Fig 5A–5C). Again we observed an increase in response that behaved in a dose-dependent and saturable manner, similar to the results obtained in Fig 4B–4D. Likewise, only the initial association rate k_{a1} was changed, while the stability of the complex (k_{d1}), the second rate step (k_{a2} and k_{d2}), and maximum response when all the binding sites on active $\alpha_5\beta_1$ are saturated (R_{max}) were unaffected by the presence of MSCRAMMs (Fig 5B–5D). The initial

Table 2. Kinetic parameters for Fn::$\alpha_5\beta_1$ interactions.

Analyte injected	k_{a1}($\times 10^4$ $M^{-1}s^{-1}$)	k_{d1} ($\times 10^{-2}$ s^{-1})	k_{a2} ($\times 10^{-5}$ $RU^{-1}s^{-1}$)	k_{d2} ($\times 10^{-3}$ s^{-1})	K_D (nM)	χ^2
Fn alone	1.5 ± 0.0	1.5 ± 0.0	1.1 ± 0.1	0.9 ± 0.0	1000 ± 130	1.15 ± 0.26
Fn + FnBPA-10	6.1 ± 0.6	1.5 ± 0.2	1.3 ± 0.3	1.0 ± 0.1	260 ± 90	1.10 ± 0.29
Fn + BBK32	7.5 ± 0.8	1.2 ± 0.2	0.8 ± 0.0	1.0 ± 0.1	170 ± 90	1.04 ± 0.42

Association (k_{a1}, k_{a2}) and dissociation rate (k_{d1}, k_{d2}) constants obtained from fitting SPR response curves (Fig 4B–4D) to a bivalent analyte binding model. The statistical value χ^2 is also listed to show the closeness of each fit. Values are mean values (with standard error in parentheses) obtained from at least three experiments.

doi:10.1371/journal.pone.0159118.t002

association rate, k_{a1}, is the only kinetic parameter directly affected by analyte concentration (units = $M^{-1}s^{-1}$). As the concentrations of Fn used across experiments were the same, the observed increase in k_{a1} for Fn bound by increasing concentrations of MSCRAMMs likely represents an increase in the apparent concentration of the active integrin binding site in Fn.

High-affinity FnBPA/Fn-NTD interaction is required for enhancement of Fn/$\alpha_5\beta_1$ activity

Of the eleven Fn-binding repeats found in FnBPA, six have been characterized as high-affinity binders (FnBPA-1, -4, -5, -9, -10, -11). The higher affinity of these repeats has been attributed to their ability to interact with four sequential FnI modules of the Fn-NTD fragment [46]. For example, while FnBPA-10 contains correctly spaced motifs to interact with $^{2\text{-}5}$FnI in a β-tandem zipper model of binding, the low-affinity repeat FnBPA-3 appears to lack the ^{5}FnI interaction motif. Intriguingly, these particular Fn modules have been implicated in mediating long-range intra-molecular contacts within native Fn dimers (Fig 1A) [19,21,22]. To understand if high-affinity interaction is required for an MSCRAMM-induced increase in Fn/$\alpha_5\beta_1$ recognition, we next tested a panel of high and low-affinity FnBPA repeats (Fig 6). All high-affinity

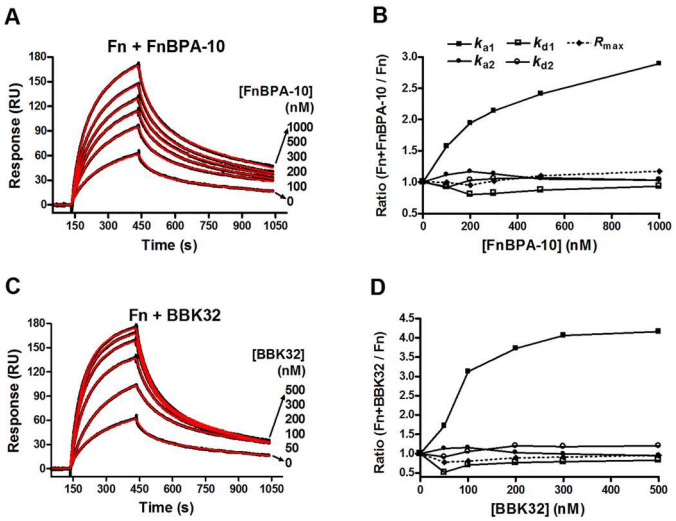

Fig 5. SPR analysis of kinetic components of the Fn/$\alpha_5\beta_1$ interaction that are affected by MSCRAMMs. Fn (50 nM) in the presence of indicated concentration of **(A)** FnBPA-10 or **(C)** BBK32 was injected over an $\alpha_5\beta_1$ surface on a Biacore sensor chip. Kinetic components (k_{a1}, k_{d1}, k_{a2}, k_{d2}) and R_{max} obtained from local fitting were normalized to those of Fn alone, and plotted as a function of **(B)** FnBPA-10 or **(D)** BBK32 concentrations.

doi:10.1371/journal.pone.0159118.g005

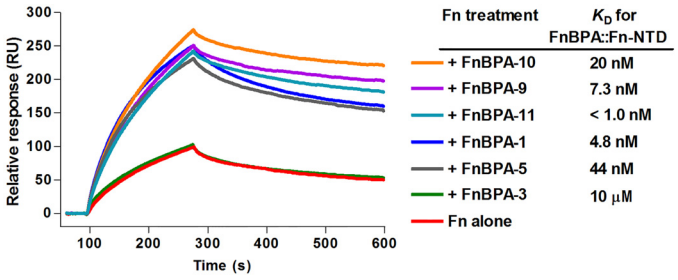

Fig 6. Relationship of high affinity Fn-NTD fragment interaction and $\alpha_5\beta_1$ integrin activation. SPR sensorgrams were generated by injecting 50 nM Fn in the presence of GST-fused FnBPA repeats (0.5 μM for high-affinity repeats -1, -5, -9, -10, -11 and 15 μM for low affinity repeat -3) over immobilized $\alpha_5\beta_1$. The K_D reported for direct binding of Fn-NTD by high affinity FnBPA repeats are provided for reference and were obtained from previously published isothermal titration calorimetry (ITC) experiments [46]. The weak affinity between FnBPA-3 and Fn-NTD was measured by SPR (this work, data not shown). None of the repeats bound directly to $\alpha_5\beta_1$ (data not shown).

doi:10.1371/journal.pone.0159118.g006

repeats studied (FnBPA-1, -5, -9, -10, and -11) increased the Fn/$\alpha_5\beta_1$ binding response, while the low-affinity repeat FnBPA-3 exhibited control-level signal.

MSCRAMMs enhance Fn/$\alpha_5\beta_1$ interaction in human plasma

The SPR-based activity assay utilizing purified native and recombinant reagents allowed for a quantitative kinetic assessment of the MSCRAMM-induced enhancement of Fn/$\alpha_5\beta_1$ binding. We next asked if this effect could be recapitulated using human plasma as a source of native Fn. Indeed, an MSCRAMM-dependent increase in plasma Fn/$\alpha_5\beta_1$ binding was observed in the presence of FnBPA-10 or and to a greater extent for BBK32 when 5% human plasma (~15 μg ml^{-1} or equivalently ~30 nM Fn) was used in an ELISA-type binding assay (Fig 7).

Discussion

Modeling the allosteric activation of Fn/$\alpha_5\beta_1$ by Fn-binding MSCRAMMs

By manipulating the conformation of key Fn functional domains, Fn-binding MSCRAMMs enable pathogens to hijack normal host physiology. In the case of *S. aureus*, enhanced Fn/$\alpha_5\beta_1$ interaction leads to recruitment of focal contact-associated proteins and subsequent integrin clustering at the bacterial attachment site initiates intracellular signaling through the focal adhesion kinase (FAK) and Src kinases [33,43,75]. This appears to confer an advantage to *S. aureus* by facilitating immune evasion and serves as a bacterial reservoir in chronic infections

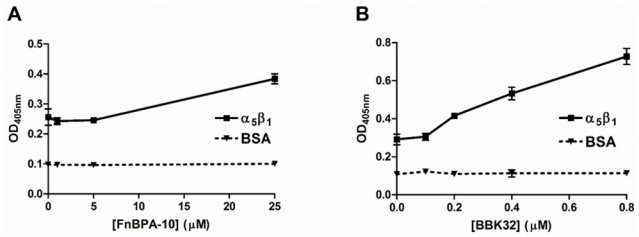

Fig 7. ELISA detection of the effect of MSCRAMMs on intact Fn in plasma for $\alpha_5\beta_1$ binding. 5% human blood plasma in TBS containing 1 mM $MnCl_2$ was incubated with **(A)** FnBPA-10 or **(B)** BBK32, and added $\alpha_5\beta_1$-coated wells or BSA (0.2 μg per well) coated surfaces. Bound Fn was probed with anti-Fn pAb. BBK32 did not bind directly to $\alpha_5\beta_1$ when detected by anti-BBK32 pAb (data not shown). Data are one representative of three experiments.

doi:10.1371/journal.pone.0159118.g007

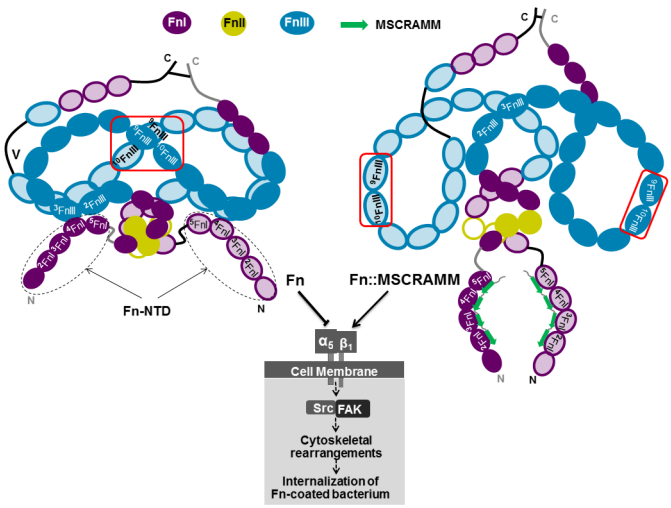

Fig 8. An allosteric model of Fn activation by MSCRAMMs. Based on the data presented here and the previously proposed allosteric model of Fn activation by streptococcal and borrelial FnBPs [6,12,17], we constructed the above model for allosteric affinity enhancement of the Fn/$\alpha_5\beta_1$ interaction by staphylococcal FnBPA. Fn is represented in its native state (left) or bound by FnBPA (right). The native Fn model including intermolecular contacts are adapted from a previously proposed model based on multiple independent studies. In a native state, major solution conformations of Fn occlude the canonical $\alpha_5\beta_1$ interaction motifs located in $^{9\text{-}10}$FnIII domains. Upon binding to Fn, FnBPA disrupts specific intermolecular contacts in the N-terminal domain of Fn (Fn-NTD) resulting in global structural rearrangements at sites distant from the FnBPA binding site. Previously cryptic integrin interaction sites are exposed, promoting interaction of Fn with $\alpha_5\beta_1$. This initiates 'outside-in' signaling events leading to cytoskeletal rearrangement and eventual internalization of Fn-coated *S. aureus*.

doi:10.1371/journal.pone.0159118.g008

[33,51]. In light of the observations above, we propose a model for the allosteric enhancement of Fn/$\alpha_5\beta_1$ binding by staphylococcal FnBPA (Fig 8), similar to that put forward for streptococcal and borrelial FnBPs [6,12,13,17]. We speculate that dimeric native Fn exists as an array of conformers in solution. At equilibrium, predominate forms of Fn are compact and sterically occlude $\alpha_5\beta_1$ interaction domains (^{9}FnIII-^{10}FnIII) by long-range intramolecular interactions, thereby impeding Fn/$\alpha_5\beta_1$ recognition. The equilibrium of Fn conformers shifts upon high-affinity binding of FnBPA and native intramolecular contacts are disrupted exposing previously cryptic $\alpha_5\beta_1$ binding sites and promoting Fn/$\alpha_5\beta_1$ binding. Domains involved in integrin binding by Fn are located at a site distant from the MSCRAMM binding site. It appears then that a critical feature of MSCRAMM-induced activation of Fn/$\alpha_5\beta_1$ is allostery and allosteric modes of host protein modulation have been previously reported for *S. aureus* [76]. Our findings also suggest that the conformation of integrin ligands, like Fn, may fine-tune affinities and therefore contribute to integrin "activation" traditionally associated with conformational change of the integrin ectodomains [77].

The data presented here provides a foundation to study the potential involvement of Fn-binding MSCRAMMs in several aspects of Fn physiology. In addition to Fn/integrin interaction, cryptic functional sites in Fn play a fundamental role in mechanoresponsive and motogenic pathways [19,78]. Interestingly, polymorphisms have been recently reported in two high-affinity FnBPA repeats (FnBPA-5 and -9) and *S. aureus* strains harboring these mutations are highly correlated with infection of cardiovascular devices [79,80]. How these FnBPA mutations impact bound Fn tertiary structure is currently unknown, however, we predict that sequence changes to residues in FnBPA repeats could result in different global Fn structure and thus function. Finally, as the clinical relevance of intracellular forms of *S. aureus* are becoming

clearer [51], elucidation of the molecular mechanisms of Fn-binding MSCRAMMs, like FnBPA, stands to provide a major contribution towards improving the treatment of staphylococcal infectious diseases.

Supporting Information

S1 Fig. Steady-state fluorescence spectroscopy. Intrinsic tryptophan fluorescence spectra of Fn solutions were obtained on a Spectrofluorimeter LS 50B (Perkin-Elmer) at ambient temperature. (**A**) Fn (0.1 μM) was incubated in TBS in the presence of 1 M GdnHCl, 0.2 μM BBK32 or 2 μM of FnBPA-10. (**B**) FnNTD-30K (1.6 μM) were incubated in TBS in the presence of 16 μM of FnBPA-10. Samples were excited at 295 nm with and excitation slit of 5 nm, and emission spectra were collected with an emission slit of 5 nm. All spectra were corrected for background fluorescence by subtraction of the buffer blanks.
(TIF)

S2 Fig. SPR analysis of Fn/$\alpha_5\beta_1$ interaction. The $\alpha_5\beta_1$ biosensor was validated by demonstrating metal ion dependence and domain specificity: **(A)** Fn (250 nM) was injected over immobilized $\alpha_5\beta_1$ surface in the presence of 1 mM $MnCl_2$ (solid line) or 3 mM EDTA (dashed line). **(B)** Response curves for a two-fold linear dilution series of Fn-CBD over immobilized $\alpha_5\beta_1$ are shown. **(C)** Comparison of Fn (250 nM, solid line) and the Fn-NTD fragment lacking the canonical integrin binding RGD-motif (500 nM, dashed line).
(TIFF)

Acknowledgments

The authors are grateful for Susan E. Craig from the Wellcome Trust Centre for CellMatrix Research at University of Manchester for the recombinant integrin $\alpha_5\beta_1$.

Author Contributions

Conceived and designed the experiments: MH XL. Performed the experiments: XL. Analyzed the data: MH XL BLG. Contributed reagents/materials/analysis tools: SP LV NAGM MJH JRP. Wrote the paper: MH XL BLG.

References

1. Leiss M, Beckmann K, Giros A, Costell M, Fassler R. The role of integrin binding sites in fibronectin matrix assembly in vivo. Curr Opin Cell Biol. 2008; 20: 502–507. doi: 10.1016/j.ceb.2008.06.001 PMID: 18586094
2. Henderson B, Nair S, Pallas J, Williams MA. Fibronectin: a multidomain host adhesin targeted by bacterial fibronectin-binding proteins. FEMS Microbiol Rev. 2011; 35: 147–200. doi: 10.1111/j.1574-6976.2010.00243.x PMID: 20695902
3. Moretti FA, Chauhan AK, Iaconcig A, Porro F, Baralle FE, Muro AF. A major fraction of fibronectin present in the extracellular matrix of tissues is plasma-derived. J Biol Chem. 2007; 282: 28057–28062. M611315200 [pii]. PMID: 17644525
4. To WS, Midwood KS. Plasma and cellular fibronectin: distinct and independent functions during tissue repair. Fibrogenesis Tissue Repair. 2011; 4: 21-1536-4-21. doi: 10.1186/1755-1536-4-21
5. Peters JH, Loredo GA, Chen G, Maunder R, Hahn TJ, Willits NH, et al. Plasma levels of fibronectin bearing the alternatively spliced EIIIB segment are increased after major trauma. J Lab Clin Med. 2003; 141: 401–410. doi: 10.1016/S0022-2143(03)00042-8 PMID: 12819638
6. Harris G, Ma W, Maurer LM, Potts JR, Mosher DF. Borrelia burgdorferi protein BBK32 binds to soluble fibronectin via the N-terminal 70-kDa region, causing fibronectin to undergo conformational extension. J Biol Chem. 2014; 289: 22490–22499. doi: 10.1074/jbc.M114.578419 PMID: 24962582

7. Garcia BL, Zhi H, Wager B, Hook M, Skare JT. Borrelia burgdorferi BBK32 Inhibits the Classical Pathway by Blocking Activation of the C1 Complement Complex. PLoS Pathog. 2016; 12: e1005404. doi: 10.1371/journal.ppat.1005404 PMID: 26808924
8. Heying R, van de Gevel J, Que YA, Moreillon P, Beekhuizen H. Fibronectin-binding proteins and clumping factor A in Staphylococcus aureus experimental endocarditis: FnBPA is sufficient to activate human endothelial cells. Thromb Haemost. 2007; 97: 617–626. 07040617 [pii]. PMID: 17393025
9. Fisher M, Huang YS, Li X, McIver KS, Toukoki C, Eichenbaum Z. Shr is a broad-spectrum surface receptor that contributes to adherence and virulence in group A streptococcus. Infect Immun. 2008; 76: 5006–5015. doi: 10.1128/IAI.00300-08 PMID: 18710861
10. Brouillette E, Talbot BG, Malouin F. The fibronectin-binding proteins of Staphylococcus aureus may promote mammary gland colonization in a lactating mouse model of mastitis. Infect Immun. 2003; 71: 2292–2295. PMID: 12654860
11. Marjenberg ZR, Ellis IR, Hagan RM, Prabhakaran S, Hook M, Talay SR, et al. Cooperative binding and activation of fibronectin by a bacterial surface protein. J Biol Chem. 2011; 286: 1884–1894. doi: 10.1074/jbc.M110.183053 PMID: 21059652
12. Maurer LM, Ma W, Eickstaedt NL, Johnson IA, Tomasini-Johansson BR, Annis DS, et al. Ligation of the fibrin-binding domain by beta-strand addition is sufficient for expansion of soluble fibronectin. J Biol Chem. 2012; 287: 13303–13312. doi: 10.1074/jbc.M111.294041 PMID: 22351755
13. Maurer LM, Tomasini-Johansson BR, Ma W, Annis DS, Eickstaedt NL, Ensenberger MG, et al. Extended binding site on fibronectin for the functional upstream domain of protein F1 of Streptococcus pyogenes. J Biol Chem. 2010; 285: 41087–41099. doi: 10.1074/jbc.M110.153692 PMID: 20947497
14. Edwards AM, Potts JR, Josefsson E, Massey RC. Staphylococcus aureus host cell invasion and virulence in sepsis is facilitated by the multiple repeats within FnBPA. PLoS Pathog. 2010; 6: e1000964. doi: 10.1371/journal.ppat.1000964 PMID: 20585570
15. Edwards AM, Potter U, Meenan NA, Potts JR, Massey RC. Staphylococcus aureus keratinocyte invasion is dependent upon multiple high-affinity fibronectin-binding repeats within FnBPA. PLoS One. 2011; 6: e18899. doi: 10.1371/journal.pone.0018899 PMID: 21526122
16. Massey RC, Kantzanou MN, Fowler T, Day NP, Schofield K, Wann ER, et al. Fibronectin-binding protein A of Staphylococcus aureus has multiple, substituting, binding regions that mediate adherence to fibronectin and invasion of endothelial cells. Cell Microbiol. 2001; 3: 839–851. 157 [pii]. PMID: 11736995
17. Ensenberger MG, Annis DS, Mosher DF. Actions of the functional upstream domain of protein F1 of Streptococcus pyogenes on the conformation of fibronectin. Biophys Chem. 2004; 112: 201–207. S0301-4622(04)00188-7 [pii]. PMID: 15572249
18. Nelea V, Nakano Y, Kaartinen MT. Size distribution and molecular associations of plasma fibronectin and fibronectin crosslinked by transglutaminase 2. Protein J. 2008; 27: 223–233. doi: 10.1007/s10930-008-9128-1 PMID: 18330684
19. Vakonakis I, Staunton D, Ellis IR, Sarkies P, Flanagan A, Schor AM, et al. Motogenic sites in human fibronectin are masked by long range interactions. J Biol Chem. 2009; 284: 15668–15675. doi: 10.1074/jbc.M109.003673 PMID: 19366708
20. Johnson KJ, Sage H, Briscoe G, Erickson HP. The compact conformation of fibronectin is determined by intramolecular ionic interactions. J Biol Chem. 1999; 274: 15473–15479. PMID: 10336438
21. Bultmann H, Santas AJ, Peters DM. Fibronectin fibrillogenesis involves the heparin II binding domain of fibronectin. J Biol Chem. 1998; 273: 2601–2609. PMID: 9446562
22. Homandberg GA, Erickson JW. Model of fibronectin tertiary structure based on studies of interactions between fragments. Biochemistry. 1986; 25: 6917–6925. PMID: 3801402
23. Raibaud S, Schwarz-Linek U, Kim JH, Jenkins HT, Baines ER, Gurusiddappa S, et al. Borrelia burgdorferi binds fibronectin through a tandem beta-zipper, a common mechanism of fibronectin binding in staphylococci, streptococci, and spirochetes. J Biol Chem. 2005; 280: 18803–18809. M501731200 [pii]. PMID: 15737988
24. Norris NC, Bingham RJ, Harris G, Speakman A, Jones RP, Leech A, et al. Structural and functional analysis of the tandem beta-zipper interaction of a Streptococcal protein with human fibronectin. J Biol Chem. 2011; 286: 38311–38320. doi: 10.1074/jbc.M111.276592 PMID: 21840989
25. Schwarz-Linek U, Werner JM, Pickford AR, Gurusiddappa S, Kim JH, Pilka ES, et al. Pathogenic bacteria attach to human fibronectin through a tandem beta-zipper. Nature. 2003; 423: 177–181. doi: 10.1038/nature01589 PMID: 12736686
26. Ugarova TP, Zamarron C, Veklich Y, Bowditch RD, Ginsberg MH, Weisel JW, et al. Conformational transitions in the cell binding domain of fibronectin. Biochemistry. 1995; 34: 4457–4466. PMID: 7535564

27. Ma W, Ma H, Fogerty FJ, Mosher DF. Bivalent ligation of the collagen-binding modules of fibronectin by SFS, a non-anchored bacterial protein of Streptococcus equi. J Biol Chem. 2015; 290: 4866–4876. doi: 10.1074/jbc.M114.612259 PMID: 25525266

28. Hynes RO. Integrins: bidirectional, allosteric signaling machines. Cell. 2002; 110: 673–687. S0092867402009716 [pii]. PMID: 12297042

29. Hauck CR, Borisova M, Muenzner P. Exploitation of integrin function by pathogenic microbes. Curr Opin Cell Biol. 2012; 24: 637–644. doi: 10.1016/j.ceb.2012.07.004 PMID: 22884865

30. Coburn J, Chege W, Magoun L, Bodary SC, Leong JM. Characterization of a candidate Borrelia burgdorferi beta3-chain integrin ligand identified using a phage display library. Mol Microbiol. 1999; 34: 926–940. mmi1654 [pii]. PMID: 10594819

31. Kwok T, Zabler D, Urman S, Rohde M, Hartig R, Wessler S, et al. Helicobacter exploits integrin for type IV secretion and kinase activation. Nature. 2007; 449: 862–866. nature06187 [pii]. PMID: 17943123

32. Isberg RR, Leong JM. Multiple beta 1 chain integrins are receptors for invasin, a protein that promotes bacterial penetration into mammalian cells. Cell. 1990; 60: 861–871. 0092-8674(90)90099-Z [pii]. PMID: 2311122

33. Hauck CR, Ohlsen K. Sticky connections: extracellular matrix protein recognition and integrin-mediated cellular invasion by Staphylococcus aureus. Curr Opin Microbiol. 2006; 9: 5–11. S1369-5274(05)00196-7 [pii]. PMID: 16406780

34. Hoffmann C, Ohlsen K, Hauck CR. Integrin-mediated uptake of fibronectin-binding bacteria. Eur J Cell Biol. 2011; 90: 891–896. doi: 10.1016/j.ejcb.2011.03.001 PMID: 21561684

35. Foster TJ, Hook M. Surface protein adhesins of Staphylococcus aureus. Trends Microbiol. 1998; 6: 484–488. S0966-842X(98)01400-0 [pii]. PMID: 10036727

36. Sinha B, Francois PP, Nusse O, Foti M, Hartford OM, Vaudaux P, et al. Fibronectin-binding protein acts as Staphylococcus aureus invasin via fibronectin bridging to integrin alpha5beta1. Cell Microbiol. 1999; 1: 101–117. cmi11 [pii]. PMID: 11207545

37. Dziewanowska K, Patti JM, Deobald CF, Bayles KW, Trumble WR, Bohach GA. Fibronectin binding protein and host cell tyrosine kinase are required for internalization of Staphylococcus aureus by epithelial cells. Infect Immun. 1999; 67: 4673–4678. PMID: 10456915

38. Lammers A, Nuijten PJ, Smith HE. The fibronectin binding proteins of Staphylococcus aureus are required for adhesion to and invasion of bovine mammary gland cells. FEMS Microbiol Lett. 1999; 180: 103–109. S0378-1097(99)00470-X [pii]. PMID: 10547450

39. Fowler T, Wann ER, Joh D, Johansson S, Foster TJ, Hook M. Cellular invasion by Staphylococcus aureus involves a fibronectin bridge between the bacterial fibronectin-binding MSCRAMMs and host cell beta1 integrins. Eur J Cell Biol. 2000; 79: 672–679. PMID: 11089915

40. Schroder A, Schroder B, Roppenser B, Linder S, Sinha B, Fassler R, et al. Staphylococcus aureus fibronectin binding protein-A induces motile attachment sites and complex actin remodeling in living endothelial cells. Mol Biol Cell. 2006; 17: 5198–5210. E06-05-0463 [pii]. PMID: 17021255

41. Sinha B, Francois P, Que YA, Hussain M, Heilmann C, Moreillon P, et al. Heterologously expressed Staphylococcus aureus fibronectin-binding proteins are sufficient for invasion of host cells. Infect Immun. 2000; 68: 6871–6878. PMID: 11083807

42. Sinha B, Herrmann M. Mechanism and consequences of invasion of endothelial cells by Staphylococcus aureus. Thromb Haemost. 2005; 94: 266–277. 05080266 [pii]. PMID: 16113815

43. Agerer F, Lux S, Michel A, Rohde M, Ohlsen K, Hauck CR. Cellular invasion by Staphylococcus aureus reveals a functional link between focal adhesion kinase and cortactin in integrin-mediated internalisation. J Cell Sci. 2005; 118: 2189–2200. jcs.02328 [pii]. PMID: 15855238

44. Shinji H, Yosizawa Y, Tajima A, Iwase T, Sugimoto S, Seki K, et al. Role of fibronectin-binding proteins A and B in in vitro cellular infections and in vivo septic infections by Staphylococcus aureus. Infect Immun. 2011; 79: 2215–2223. doi: 10.1128/IAI.00133-11 PMID: 21422173

45. Kerdudou S, Laschke MW, Sinha B, Preissner KT, Menger MD, Herrmann M. Fibronectin binding proteins contribute to the adherence of Staphylococcus aureus to intact endothelium in vivo. Thromb Haemost. 2006; 96: 183–189. 06080183 [pii]. PMID: 16894462

46. Meenan NA, Visai L, Valtulina V, Schwarz-Linek U, Norris NC, Gurusiddappa S, et al. The tandem beta-zipper model defines high affinity fibronectin-binding repeats within Staphylococcus aureus FnBPA. J Biol Chem. 2007; 282: 25893–25902. M703063200 [pii]. PMID: 17606607

47. Bosse MJ, Gruber HE, Ramp WK. Internalization of bacteria by osteoblasts in a patient with recurrent, long-term osteomyelitis. A case report. J Bone Joint Surg Am. 2005; 87: 1343–1347. 87/6/1343 [pii]. PMID: 15930546

48. Clement S, Vaudaux P, Francois P, Schrenzel J, Huggler E, Kampf S, et al. Evidence of an intracellular reservoir in the nasal mucosa of patients with recurrent Staphylococcus aureus rhinosinusitis. J Infect Dis. 2005; 192: 1023–1028. JID34531 [pii]. PMID: 16107955

49. Jarry TM, Memmi G, Cheung AL. The expression of alpha-haemolysin is required for Staphylococcus aureus phagosomal escape after internalization in CFT-1 cells. Cell Microbiol. 2008; 10: 1801–1814. doi: 10.1111/j.1462-5822.2008.01166.x PMID: 18466345

50. Que YA, Haefliger JA, Piroth L, Francois P, Widmer E, Entenza JM, et al. Fibrinogen and fibronectin binding cooperate for valve infection and invasion in Staphylococcus aureus experimental endocarditis. J Exp Med. 2005; 201: 1627–1635. jem.20050125 [pii]. PMID: 15897276

51. Lehar SM, Pillow T, Xu M, Staben L, Kajihara KK, Vandlen R, et al. Novel antibody-antibiotic conjugate eliminates intracellular S. aureus. Nature. 2015; 527: 323–328. doi: 10.1038/nature16057 PMID: 26536114

52. Speziale P, Visai L, Rindi S, Di Poto A. Purification of human plasma fibronectin using immobilized gelatin and Arg affinity chromatography. Nat Protoc. 2008; 3: 525–533. doi: 10.1038/nprot.2008.12 PMID: 18323821

53. Coe AP, Askari JA, Kline AD, Robinson MK, Kirby H, Stephens PE, et al. Generation of a minimal alpha5beta1 integrin-Fc fragment. J Biol Chem. 2001; 276: 35854–35866. doi: 10.1074/jbc.M103639200 PMID: 11389148

54. Zardi L, Carnemolla B, Balza E, Borsi L, Castellani P, Rocco M, et al. Elution of fibronectin proteolytic fragments from a hydroxyapatite chromatography column. A simple procedure for the purification of fibronectin domains. Eur J Biochem. 1985; 146: 571–579. PMID: 2982601

55. Prabhakaran S, Liang X, Skare JT, Potts JR, Hook M. A novel fibronectin binding motif in MSCRAMMs targets F3 modules. PLoS One. 2009; 4: e5412. doi: 10.1371/journal.pone.0005412 PMID: 19404402

56. Baneyx G, Baugh L, Vogel V. Coexisting conformations of fibronectin in cell culture imaged using fluorescence resonance energy transfer. Proc Natl Acad Sci U S A. 2001; 98: 14464–14468. doi: 10.1073/pnas.251422998 PMID: 11717404

57. Williams EC, Janmey PA, Ferry JD, Mosher DF. Conformational states of fibronectin. Effects of pH, ionic strength, and collagen binding. J Biol Chem. 1982; 257: 14973–14978. PMID: 7174679

58. Rocco M, Carson M, Hantgan R, McDonagh J, Hermans J. Dependence of the shape of the plasma fibronectin molecule on solvent composition. Ionic strength and glycerol content. J Biol Chem. 1983; 258: 14545–14549. PMID: 6643501

59. Lai CS, Wolff CE, Novello D, Griffone L, Cuniberti C, Molina F, et al. Solution structure of human plasma fibronectin under different solvent conditions. Fluorescence energy transfer, circular dichroism and light-scattering studies. J Mol Biol. 1993; 230: 625–640. S0022-2836(83)71174-5 [pii]. PMID: 8464068

60. Pelta J, Berry H, Fadda GC, Pauthe E, Lairez D. Statistical conformation of human plasma fibronectin. Biochemistry. 2000; 39: 5146–5154. bi992770x [pii]. PMID: 10819982

61. Pauthe E, Pelta J, Patel S, Lairez D, Goubard F. Temperature-induced beta-aggregation of fibronectin in aqueous solution. Biochim Biophys Acta. 2002; 1597: 12–21. S0167483802002716 [pii]. PMID: 12009397

62. Lai CS, Tooney NM, Ankel EG. Structure and flexibility of plasma fibronectin in solution: electron spin resonance spin-label, circular dichroism, and sedimentation studies. Biochemistry. 1984; 23: 6393–6397. PMID: 6099139

63. Patel S, Chaffotte AF, Goubard F, Pauthe E. Urea-induced sequential unfolding of fibronectin: a fluorescence spectroscopy and circular dichroism study. Biochemistry. 2004; 43: 1724–1735. doi: 10.1021/bi0347104 PMID: 14769050

64. Benecky MJ, Kolvenbach CG, Wine RW, DiOrio JP, Mosesson MW. Human plasma fibronectin structure probed by steady-state fluorescence polarization: evidence for a rigid oblate structure. Biochemistry. 1990; 29: 3082–3091. PMID: 2337580

65. Sjoberg B, Pap S, Osterlund E, Osterlund K, Vuento M, Kjems J. Solution structure of human plasma fibronectin using small-angle X-ray and neutron scattering at physiological pH and ionic strength. Arch Biochem Biophys. 1987; 255: 347–353. PMID: 3592678

66. Lairez D, Pauthe E, Pelta J. Refolding of a high molecular weight protein: salt effect on collapse. Biophys J. 2003; 84: 3904–3916. S0006-3495(03)75118-2 [pii]. PMID: 12770896

67. Alexander SS Jr, Colonna G, Edelhoch H. The structure and stability of human plasma cold-insoluble globulin. J Biol Chem. 1979; 254: 1501–1505. PMID: 762148

68. Osterlund E, Eronen I, Osterlund K, Vuento M. Secondary structure of human plasma fibronectin: conformational change induced by calf alveolar heparan sulfates. Biochemistry. 1985; 24: 2661–2667. PMID: 3161537

69. Khan MY, Medow MS, Newman SA. Unfolding transitions of fibronectin and its domains. Stabilization and structural alteration of the N-terminal domain by heparin. Biochem J. 1990; 270: 33–38. PMID: 2396990

70. Brumfeld V, Werber MM. Studies on fibronectin and its domains. II. Secondary structure and spatial configuration of fibronectin and of its domains. Arch Biochem Biophys. 1993; 302: 134–143. S0003-9861(83)71191-4 [pii]. PMID: 8470891

71. Wolff CE, Lai CS. Inter-sulfhydryl distances in plasma fibronectin determined by fluorescence energy transfer: effect of environmental factors. Biochemistry. 1990; 29: 3354–3361. PMID: 2334697

72. Takagi J, Strokovich K, Springer TA, Walz T. Structure of integrin alpha5beta1 in complex with fibronectin. EMBO J. 2003; 22: 4607–4615. doi: 10.1093/emboj/cdg445 PMID: 12970173

73. Campbell ID, Humphries MJ. Integrin structure, activation, and interactions. Cold Spring Harb Perspect Biol. 2011; 3: doi: 10.1101/cshperspect.a004994

74. Akiyama SK, Hasegawa E, Hasegawa T, Yamada KM. The interaction of fibronectin fragments with fibroblastic cells. J Biol Chem. 1985; 260: 13256–13260. PMID: 2932436

75. Fraunholz M, Sinha B. Intracellular Staphylococcus aureus: live-in and let die. Front Cell Infect Microbiol. 2012; 2: 43. doi: 10.3389/fcimb.2012.00043 PMID: 22919634

76. Chen H, Ricklin D, Hammel M, Garcia BL, McWhorter WJ, Sfyroera G, et al. Allosteric inhibition of complement function by a staphylococcal immune evasion protein. Proc Natl Acad Sci U S A. 2010; 107: 17621–17626. doi: 10.1073/pnas.1003750107 PMID: 20876141

77. Shattil SJ, Kim C, Ginsberg MH. The final steps of integrin activation: the end game. Nat Rev Mol Cell Biol. 2010; 11: 288–300. doi: 10.1038/nrm2871 PMID: 20308986

78. Vogel V. Mechanotransduction involving multimodular proteins: converting force into biochemical signals. Annu Rev Biophys Biomol Struct. 2006; 35: 459–488. doi: 10.1146/annurev.biophys.35.040405.102013 PMID: 16689645

79. Lower SK, Lamlertthon S, Casillas-Ituarte NN, Lins RD, Yongsunthon R, Taylor ES, et al. Polymorphisms in fibronectin binding protein A of Staphylococcus aureus are associated with infection of cardiovascular devices. Proc Natl Acad Sci U S A. 2011; 108: 18372–18377. doi: 10.1073/pnas.1109071108 PMID: 22025727

80. Xiong YQ, Sharma-Kuinkel BK, Casillas-Ituarte NN, Fowler VG Jr, Rude T, DiBartola AC, et al. Endovascular infections caused by methicillin-resistant Staphylococcus aureus are linked to clonal complex-specific alterations in binding and invasion domains of fibronectin-binding protein A as well as the occurrence of fnbB. Infect Immun. 2015; 83: 4772–4780. doi: 10.1128/IAI.01074-15 PMID: 26416903